Mechanism of Micro Manipulation using Oscillation

メタデータ	言語: eng
	出版者:
	公開日: 2017-10-03
	キーワード (Ja):
	キーワード (En):
	作成者:
	メールアドレス:
	所属:
URL	http://hdl.handle.net/2297/35231

Mechanism of Micro Manipulation using Oscillation

Tetsuyou Watanabe
Dep. of Mech. Eng.
Yamaguchi University
Ube, 755-8611, Japan
Email: te-watanabe@ieee.org

Zhongwei Jiang
Dep. of Mech. Eng.
Yamaguchi University
Ube, 755-8611, Japan
Email: jiang@yamaguchi-u.ac.jp

Abstract— In this paper, we analyze the mechanism of the phenomenon between an endeffector, a micro object and a substrate during a micro manipulation. In a micro range, the attracting forces such as the van der Waals, capillary, and electrostatic forces dominate and course adhesion between the object and the endeffector. The adhesion makes the manipulation of an object difficult. Recently, we developed a method to reduce the attracting/adhesion effect. When bringing an oscillating endeffector close to a micro object on a substrate, the attracting force between the object and the endeffector is reduced, attracting the object to the substrate. Then, it becomes easy to remove the endeffector from the object. Using this method, a micro object can be easily manipulated. However, the mechanism of the phenomenon is still unclear. In this paper, we develop the theoretical model of the system to analyze the phenomenon, and simulate the dynamical motion of the system. Comparing the experimental results, we show the validity of our approach. Using simulation and experiment, we show that the oscillation of the endeffector can reduce the adhesion effect between the endeffector and the object, attracting the object to the substrate.

I. Introduction

Recently, there has been a growing interest in a manipulation of a micro/nano sized object. It is the technology required to assemble or maintain microcomputers, micro electronics parts, a micro medical equipment, and so on. Different from a manipulation in a macro range, we cannot neglect an adhesion force between a micro object and an endeffector. In a macro range, the van der Waals, capillary, and electrostatic forces (proportional to surface area) become more significant than the inertial and gravitational forces (proportional to volume), because of a scale effect [1], [2]. These attracting forces (van der Waals, capillary, and electrostatic forces) cause the adhesion between a micro object and an endeffector. Therefore, even a basic operation such as pick and place becomes very hard to complete. Especially, a release of an object from an endeffector is very difficult.

Many researchers have discussed how to release a micro object [3]–[9]. Arai et. al. [3] proposed an adhesion-type micro endeffector. There are micro holes on the endeffector. By controlling the pressure inside the holes by temperature, we can absorb and release a micro object. But it is hard to control the temperature because the temperature is influenced by an environment. Also treatable objects depend on the size of the holes. Zesch et. al. [4] developed a vacuum gripping tool consisting of a glass pipette and a computer controlled

vacuum supply. But treatable objects depend on the size of a hole of the pipette. Rollot et. al. [5] proposed a method for pick and place of a micro spherical object when an endeffector has higher surface energy than a table (substrate). The problem is the release of the object. The release was done by slopping the endeffector. But the strategy can be applied to limited objects. Then, Haliyo et. al. [6], [7] proposed a strategy for the release, which is to oscillate the endeffector and give the micro object enough acceleration to remove it from the endeffector. However, it is hard to control the motion of the object after the release. Hence, to accurately position the object is very difficult. Saito et. al. [8] proposed a method for pick and place of a micro object under an SEM. But, they develop this method under the assumption that all the parameters about environment, object, and endeffector are completely known. Then, it is not easy to apply the method to practical use. Also, treatable objects are limited to a sphere. Saito et. al. [9] proposed a way for detachment of an adhering micro particle from a probe by controlling the electrostatic force. But, it is hard to control the motion of the object after the detachment, and to accurately position the object.

Recently, we developed a new strategy to cope with the adhesion force [10]. When bringing an oscillating endeffector close to a micro object on a substrate, the attracting force between the object and the endeffector is reduced, attracting the object to the substrate. Then, it becomes easy to remove the endeffector from the object. Based on this strategy, we developed a sophisticated strategy for pick and place operation in a micro range, as shown in Fig.1. Using this strategy, a micro manipulation can be done like a macro manipulation. This strategy can provide an accurate manipulation. However, "what phenomenon (actually) happens (between a micro object, an endeffector, and a substrate)" was not discussed. Therefore, we do not understand; how does the endeffector move?, how does the object move?, why the strategy is effective for reducing the attracting/adhesion effect?, and so on.

In this paper, we develop a theoretical model of the phenomenon between a micro object, an endeffector, and a substrate during a micro manipulation using the our strategy [10]. We focus on the phenomenon in the case where bringing an oscillating endeffector close to a micro object on a substrate (see Fig.1 (h)~ Fig.1 (i) and Fig.2). We derive the motion equations of the endeffector and the object, combining the vibration analysis for distributed-parameter systems and
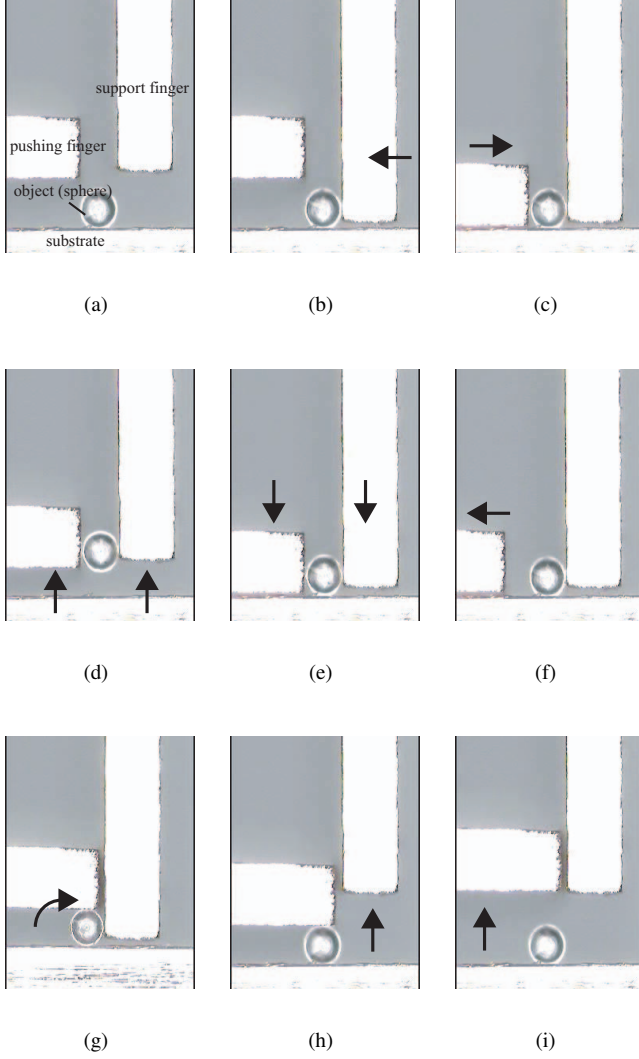
Fig. 1. Pick and place operation; (a) This is the initial state. (b) Make the support finger contact with the object on the substrate from the right side. (c) Make the oscillating pushing finger contact with the object on the substrate from the left side. The direction of the oscillation is left and right. (d) Pick the object by moving the pushing and support fingers upward. (e) Place the object by moving the pushing and support fingers downward. (f) Remove the pushing finger from the object. (g) Make the oscillating pushing finger contact with the upper side of the object. The direction of the oscillation is up and down. (h) Remove the support finger from the object by moving the support finger upward. (i) Remove the pushing finger from the object by moving the pushing finger upward. Note that in the procedure (f) and (i), the pushing finger can be easily removed from the object for the oscillation of the pushing finger, which reduces the attracting/adhesion effect.

lubrication analysis. Then, we simulate dynamical motions of the endeffector and the object. Among the attracting forces (van der Waals, capillary, and electrostatic forces), capillary force is large compared with the other forces. Therefore, the presented model includes the effect of only meniscus bridge (capillary force). Using this model, we can analyze what phenomenon does happen between a micro object, an endeffector, and a substrate, and obtain useful information for realizing stable micro manipulation. Especially, we can obtain

useful information about the object motion, which can not be measured in the experiment because of the configuration of the endeffector and the object (note that the oscillation (of the object motion) is too high to be caught by the microscope).

This paper is organized as follows. First, we present the target system, and develop a model for analyzing the phenomenon between the micro object, the endeffector, and the substrate, when bringing an oscillating endeffector close to the micro object on a substrate. Then, we simulate the dynamical motion of the object and the endeffector, and show the validity of our approach, comparing with some experimental results.

II. TARGET SYSTEM

In the manipulation shown in Fig.1, the operation is done by pushing and support fingers. The pushing finger plays a role of pushing the micro object toward the support finger and the substrate. The support finger plays a role of supporting the micro object against the pushing forces from the pushing finger. These fingers are beams, and attached on three-dimensional manipulators. On the pushing finger, a piezocell is bonded as an actuator for oscillating it. In this paper, we focus on the case when bringing the oscillating the pushing finger (hereafter, endeffector) close to the object on the substrate, which corresponds to Fig.1 (h)$\sim$ Fig.1 (i). Fig.2 shows the target system. Note that the case shown in Fig.1 (e)$\sim$ Fig.1 (f) can be analyzed by the similar way as the target case.

For the simplicity, we assume that; (1) the motion of the endeffector, the object, and the substrate is in a planner space (a gravity force doesn't work), (2) the object is a sphere, (3) the endeffector and the substrate are made by a same material, (4) among the attracting forces (van der Waals, capillary, and electrostatic forces), only capillary force is considered (because among the attracting forces, capillary force is very large compared with the other forces).

The following nomenclatures are used in this paper.

r_0 Radius of the sphere (9.7×10^{-5}[m]).
y_b Tip position of the endeffector in y direction.
y_o Position of the center of the object in y direction.
y_s Position of the substrate in y direction (1.5×10^{-7}[m]+$2r_0$).
m_o Mass of the object (9.5×10^{-9}[Kg]).
ρ Density of the endeffector (beam: 8.9×10^3[Kg/m^3], PZT: 7.65×10^3[Kg/m^3]).
$A(x)$ Cross section area of the endeffector (beam: 9.0×10^{-7}[m^2], PZT: 6.0×10^{-7}[m^2]).
$E(x)$ Young's modulus of the endeffector (beam: 10.2×10^{10}[N/m^2], PZT: 6.2×10^{10}[N/m^2]).
E_e Young's modulus of the beam (10.2×10^{10}[N/m^2]).
E_o Young's modulus of the object (7.5×10^{10}[N/m^2]).
E_s Young's modulus of the substrate (10.2×10^{10}[N/m^2]).
$I(x)$ Geometrical moment of inertia of the endeffector (beam: 6.75×10^{-15}[m^4], PZT: 2.45×10^{-14}[m^4]).
C Coefficient of structural damping of the endeffector (1.87×10^{-5}[sec]).
M_p Bending moment produced from piezocell.
l_1 Length from the root of the beam to piezocell (1[mm]).
l_2 Length of piezocell plus l_1 (3[mm]).
l Length of the beam (40[mm]).
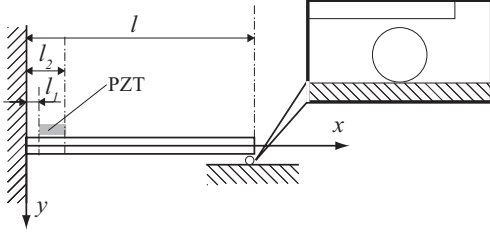l' Length from the root of the beam to the contact point with the object (0.0399[m]).

Fig. 2.   Target system

F_b Force applied to the beam resulted from the interaction between the endeffector and the object.

F_o Force applied to the object resulted from the interaction between the endeffector, the object, and the substrate.

$\delta(x)$ Dirac delta function.

$\delta'(x) = \frac{\partial \delta(x)}{\partial x}$.

P Normalized pressure of air medium between the object and the endeffector ($= p/p_a$, p: pressure between the object and the endeffector, p_a: the atmospheric pressure).

p_l Pressure of liquid medium between the object and the substrate.

R Normalized r coordinate ($= r/r_0$ where r_0 denotes the characteristic length (the radius of the sphere)).

h Thickness of the air medium between the endeffector and the object.

h_c Thickness of the air medium at the center of the contact circle between the object and the endeffector.

H Normalized thickness of air medium between the endeffector and the object ($= h/h_0$ where h_0 denotes the characteristic length ($= r_0$)).

T Normalized t (time) ($= \omega t$ where ω denotes the frequency of the oscillation).

μ Viscosity of the liquid (0.001[Pa·sec]).

μ_{air} Viscosity of the air (1.86×10^{-5}[Pa·sec]).

σ Squeeze number ($=12\mu_{air}\omega r_0^2/p_a h_0^2$).

ν_e Poisson's ratio of the beam (0.35).

ν_o Poisson's ratio of the object (0.17).

ν_s Poisson's ratio of the substrate (0.35).

γ Surface tension (73×10^{-3}[N/m] for water).

$h_{l_{eo}}$ Thickness of meniscus bridge between the endeffector and the object.

$h_{l_{eoc}}$ $h_{l_{eo}}$ at the center of the object.

$h_{l_{os}}$ Thickness of meniscus bridge between the object and the substrate.

$h_{l_{osc}}$ $h_{l_{os}}$ at the center of the object.

h_{l_e} Thickness of meniscus bridge on the endeffector (3.5[nm]).

h_{l_o} Thickness of meniscus bridge on the object (3.5[nm]).

h_{l_s} Thickness of meniscus bridge on the substrate (3.5[nm]).

θ_c Contact angle of meniscus bridge (0[rad]).

C_m Coefficient of damping when the object directly contacts with the endeffector/substrate.

r_2 the wetted radius of meniscus bridge

r_1 the meniscus curvature radius.

III. Phenomenon between a micro object, an endeffector, and a substrate

In this section, we develop a theoretical model of the phenomenon in the case when bringing an oscillating endeffecter close to a micro object on a substrate. We derive the motion equations of the endeffector and the object, combining the vibration analysis for distributed-parameter systems [11] and
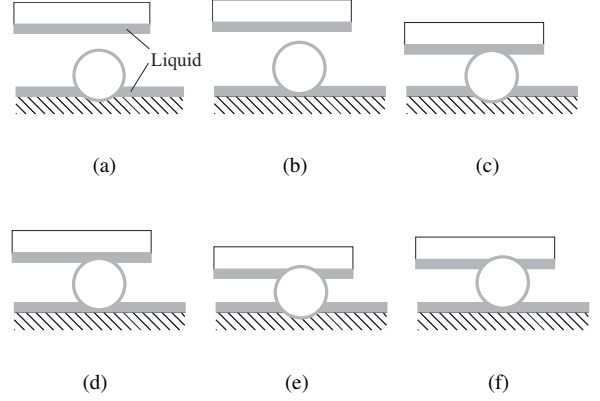

Fig. 3.   Six stages of interaction; (a) Flying-contact stage, (b) Flying-diving stage, (c) Diving-contact stage, (d) Diving-diving stage, (e) Contact-contact stage, (f) Contact-diving stage

lubrication analysis. The motion equations of the endeffector and the object, respectively, are given by:

$$\rho(x)A(x)\frac{\partial^2 y_b}{\partial t^2} + \frac{\partial^2}{\partial x^2}[E(x)I(x)(1 + C\frac{\partial}{\partial t})\frac{\partial^2 y_b}{\partial x^2}]$$
$$= M_p[\delta'(x - l_1) - \delta'(x - l_2)] + F_b\delta(x - l'), \qquad (1)$$

$$m_o\frac{\partial^2 y_o}{\partial t^2} = F_o. \qquad (2)$$

Air and liquid mediums can exist between the endeffector and the object. A liquid medium can exist between substrate and the object. Therefore, F_b and F_o vary with respect to the configuration of the endeffector, the object, and the substrate. Note that an air medium can exist between the substrate and the object. But we do not deal with the situation where the object is removed from the substrate, because the situation corresponds to end in failure of manipulation.

Here, to derive F_b and F_o, the six stages are considered, as shown in Fig.3. Flying-contact stage indicates that the endeffector interacts with the object via air medium while the object directly contacts with the substrate. Flying-diving stage indicates that the endeffector interacts with the object via air medium while the object is immersed in the liquid medium between the object and the substrate. Diving-contact stage indicates that the endeffector is immersed in the liquid medium between the object and the endeffector while the object directly contacts with the substrate. Diving-diving stage indicates that the endeffector is immersed in the liquid medium between the object and the endeffector while the object is immersed in the liquid medium between the object and the substrate. Contact-contact stage indicates that the endeffector directly contacts with the object while the object directly contacts with the substrate. Contact-diving stage indicates that the endeffector directly contacts with the object while the object is immersed in the liquid medium between the object and the substrate. In the following, we derive F_b and F_o at every stage.
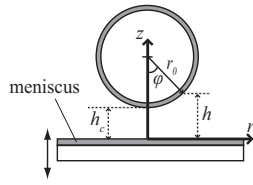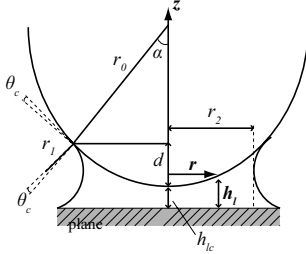
Fig. 4. Air lubrication
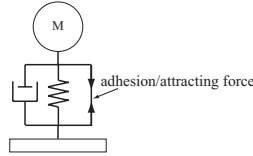

Fig. 5. liquid lubrication

Fig. 6. Contact Model

(a) Flying-contact stage

First, we consider the interaction force between the endeffector and the object, resulted from the air lubrication.

The length of the endeffector in the longitudinal direction is very large compared with the size of the object. Therefore, the surface of the endeffector around the contact/interact point with the object is assumed to be oscillated in the vertical direction to the object surface, as shown in Fig.4. As for the (air) flow, We make the following assumption; (a) The flow is Newtorian, isothermal, and a compressible perfect gas, (b) The inertia effect of the flow is negligible.

We use cylindrical coordinate. The thickness distribution of the air medium between the endeffector and the object, h, is given by (see Fig.4):

$$h = h_c + r^2/(2(r_0 + h_{l_o})). \quad (3)$$

Using h_{l_e}, h_{l_o}, y_b, y_o, and r_0, h_c is given by:

$$h_c = y_o - y_b - r_0 - h_{l_e} - h_{l_o}. \quad (4)$$

The air flow is characterized by Knudsen number K_n ($K_n = \lambda/h$ where λ denotes the molecular mean free path. $\lambda = 0.064[\mu\text{m}]$ at the atmosphere). Here, we use the generalized Reynolds equation [12]. It can be used even when the Knudsen number is large. Considering the symmetry of the system, the Reynolds equation, governing the system, is given by:

$$\frac{1}{R}\frac{\partial}{\partial R}\{PH^3 R\bar{Q}_p \frac{\partial P}{\partial R}\} = \sigma \frac{\partial(PH)}{\partial T}. \quad (5)$$

where

$$\bar{Q}_p = Q_p(D,\alpha)/Q_{con}(D), \quad Q_{con}(D) = D/6 \quad (6)$$

where $Q_p(D,\alpha)$ is a Poiseuille flow rate coefficient, $Q_{con}(D)$ is the coefficient for continuous flow, D is an inverse Knudsen number, and α is a reflection coefficient. D is expressed by

$$D = D_0 PH, \quad D_0 = p_a h_0/(\mu\sqrt{2\mathcal{R}\mathcal{T}}) \quad (7)$$

where $\mathcal{R}$ denotes the gas constant and $\mathcal{T}$ denotes the temperature. It is hard to calculate $\bar{Q}_p$. But, a data base of $\bar{Q}_p$ is developed for easy calculation [13]. The boundary conditions with respect to P are as follows; a) $P(1,T) = 1$: The pressure at the periphery is p_a at all times. b) $\frac{\partial P(0,T)}{\partial R} = 0$: The slope of the pressure profile at the center is zero at all times.

Solving (5) for P, the force exerted on the endeffector tip surface at time T is expressed by:

$$F_{air}^e = 2\pi p_a r_0^2 \int_0^1 R(P(R,T) - 1)\, dR. \quad (8)$$

Next, we consider the interaction force between the object and the substrate. Here, We assume that the contact is Hertz's contact and structural damping exists. Also, the meniscus (capillary) force is assumed to act.

First, we consider meniscus (capillary) force. In Fig.5, the following relations are obtained:

$$h_{l_{osc}} = y_s - y_o - r_0, \quad (9)$$
$$2r_1\cos(\alpha + \theta_c) = r_0(1 - \cos\alpha) + h_{l_{osc}}, \quad (10)$$
$$r_2 = r_0\cos\alpha + r_1(\sin(\alpha + \theta_c) - 1). \quad (11)$$

Note that $h_{l_{osc}} < 0$. On the other hand, r_1 and r_2 are related with the following Kelvin equation [15]):

$$(\frac{1}{r_1} + \frac{1}{r_2})^{-1} = -\frac{\mathcal{V}\gamma\cos\theta_c}{\mathcal{R}\mathcal{T}\log(p/p_0)} \quad (12)$$

where $\mathcal{V}$ denotes mole volume of the liquid (water) and p/p_0 denotes relative vapor pressure (humidity). In this stage, the object directly contacts with the substrate. The radius of the contact area is given by $\sqrt{r_0|h_{l_{osc}}|}$. Meniscus (capillary) force is assumed to act at only the area where the object contacts with the substrate via the liquid (water). Then, the meniscus (capillary) force is expressed by:

$$F_{men}^s = \pi(r_2^2 - r_0|h_{l_{osc}}|)\gamma(\frac{1}{r_1} - \frac{1}{r_2}). \quad (13)$$

In this stage, $r_1 \ll r_2$. Therefore, (12) and (13) become:

$$r_1 \cong -\frac{\mathcal{V}\gamma\cos\theta_c}{\mathcal{R}\mathcal{T}\log(p/p_0)}, \quad (14)$$
$$F_{men}^s \cong \pi(r_2^2 - r_0|h_{l_{osc}}|)\gamma/r_1. \quad (15)$$

On the other hand, the Hertz force and damping force are expressed by (see Fig.6);

$$F_{He}^s = -4/3E_{os}' r_0^{1/2}(y_o + r_0 - y_s)^{3/2}, \quad (16)$$
$$F_{dam}^s = -C_m\dot{y}_o, \quad (17)$$
$$1/E_{os}' = (1 - \nu_o^2)/E_o + (1 - \nu_s^2)/E_s,$$
$$C_m = C_{os}|\dot{y}_{o_{imp}}|, \quad (18)$$

where C_{os} is a constant, and $\dot{y}_{o_{imp}}$ denotes $\dot{y}_o$ at the instant when the collision occurs between the object and the substrate.

It is well known that the coefficient of restitution decreases with the increase of the velocity immediately before the collision. Therefore, we use (18). Note that these forces are represented as the forces applied to the object.

On the endeffector, F_{air}^{e} is exerted. On the object, F_{air}^{s}, F_{men}^{s}, F_{He}^{s}, and F_{dam}^{s} are exerted. Hence, from (8), (15), (16), and (17), F_b and F_o are given by:

$$F_b = -F_{air}^{e}, \tag{19}$$

$$F_o = F_{He}^{s} + F_{dam}^{s} + F_{men}^{s} + F_{air}^{e}. \tag{20}$$

(b) Flying-diving stage

We consider the interaction force between the object and substrate, resulted from liquid lubrication. We consider the model as shown in Fig.5. Liquid lubrication is governed by the following Reynolds equation;

$$\frac{1}{r}\frac{\partial}{\partial r}\left\{\frac{h_{l_{os}}^{3}}{12\mu_l}r\frac{\partial p_l}{\partial r}\right\} = \frac{\partial h_{l_{os}}}{\partial t}. \tag{21}$$

$h_{l_{osc}}$ is given by (10). The boundary conditions are given by: a) $\partial p_l(r = 0)/\partial r = 0$: The slope of the pressure profile at the center is zero at all times. b) $p_l(r = r_2) = -\gamma(\frac{1}{r_1} - \frac{1}{r_2})$: The pressure at the boundary of the menuscus bridge is Laplace pressure [14], [15]. r_1 and r_2 are given by (10), (11), and (12). When $r_1 \ll r_2$, r_1 and r_2 are given by (10), (11), and (14). When $\alpha \cong 0$, r_1 and r_2 are given by (12) and

$$r_1 = \frac{d + h_{l_{osc}}}{2\cos\theta_c}, \tag{22}$$

$$r_2 = \sqrt{2r_0 d}, \tag{23}$$

where

$$d = r_0(1 - \cos\alpha).$$

$h_{l_{os}}$ has the following relation with r:

$$h_{l_{os}} = h_{l_{osc}} + \frac{r^2}{2r_0}. \tag{24}$$

It is assumed that both the object and the substrates are sufficiently rigid so that the deformations of both the object and the substrates due to the interaction force are negligible. Then, the following relation is obtained:

$$\dot{h}_{l_{os}} = \dot{h}_{l_{osc}}. \tag{25}$$

From (21), (24), (25), and the boundary conditions, the following relation can be obtained:

$$p_l = -\frac{3\mu r_0 \dot{h}_{l_{osc}}}{(h_{l_{osc}} + \frac{r^2}{2r_0})^2} + \frac{3\mu r_0 \dot{h}_{l_{osc}}}{(h_{l_{osc}} + \frac{r^2}{2r_0})^2} - \gamma(\frac{1}{r_1} - \frac{1}{r_2}). \tag{26}$$

Then, the force resulted from liquid lubrication is given by:

$$F_{liq}^{s} = 2\pi \int_0^{r_2} p_l r\, dr$$

$$= -\frac{6\pi\mu r_0^2 \dot{h}_{l_{osc}}}{h_{l_{osc}}(h_{l_{osc}} + \frac{r_2^2}{2r_0})^2}\left(\frac{r_2^4}{4r_0^2} + \frac{r_2^2 h_{l_{osc}}}{r_0}\right) - \pi r_2^2 \gamma(\frac{1}{r_1} - \frac{1}{r_2}). \tag{27}$$

Here, the first term represents the damping force by a squeeze effect, and the second term represents the meniscus force.

From (8) and (27), F_b and F_o are given by:

$$F_b = -F_{air}^{e}, \tag{28}$$

$$F_o = -F_{liq}^{s} + F_{air}^{e}. \tag{29}$$

(c) Diving-contact stage

First, F_b is derived by the similar way as the derivation of F_{liq}^{s} in (27). The thickness of meniscus bridge at the center of the object, $h_{l_{eoc}}$, is given by:

$$h_{l_{eoc}} = y_o - r_o - y_b.$$

Using $h_{l_{eoc}}$, meniscus force is given by:

$$F_{liq}^{e} = -\frac{6\pi\mu r_0^2 \dot{h}_{l_{eoc}}}{h_{l_{eoc}}(h_{l_{eoc}} + \frac{r_2^2}{2r_0})^2}\left(\frac{r_2^4}{4r_0^2} + \frac{r_2^2 h_{l_{eoc}}}{r_0}\right) - \pi r_2^2 \gamma(\frac{1}{r_1} - \frac{1}{r_2}). \tag{30}$$

On the object, F_{liq}^{e}(30), F_{men}^{s}(13), F_{He}^{s}(16), and F_{dam}^{s}(17) are exerted. Therefore, F_b and F_o are given by:

$$F_b = -F_{liq}^{e} \tag{31}$$

$$F_o = F_{He}^{s} + F_{dam}^{s} + F_{men}^{s} + F_{liq}^{e}. \tag{32}$$

(d) Diving-diving stage

On the endeffector, F_{liq}^{e}(30) is exerted. On the object, F_{liq}^{e}(30) and F_{liq}^{s}(27) are exerted. Therefore, F_b and F_o are given by:

$$F_b = -F_{liq}^{e}, \tag{33}$$

$$F_o = -F_{liq}^{s} + F_{liq}^{e}. \tag{34}$$

(e) Contact-contact stage

First, the interaction force between the endeffector and the object is derived by the similar way as the derivation of F_{men}, F_{He}, and F_{dam} in (13), (16), and (17). F_b is given by:

$$F_b = F_{He}^{e} + F_{dam}^{e} + F_{men}^{e}, \tag{35}$$

$$F_{men}^{e} = \pi(r_2^2 - r_0|h_{l_{eoc}}|)\gamma(\frac{1}{r_1} - \frac{1}{r_2}). \tag{36}$$

$$F_{He}^{e} = -4/3E_{eo}^{'}r_o^{1/2}(y_b - y_o + r_0)^{3/2}, \tag{37}$$

$$F_{dam}^{e} = -C_m^{e}(\dot{y}_b - \dot{y}_o), \tag{38}$$

$$1/E_{eo}^{'} = (1 - \nu_e^2)/E_e + (1 - \nu_o^2)/E_o,$$

$$C_m^{e} = C_{eo}|\dot{y}_{b_{imp}} - \dot{y}_{o_{imp}}|, \tag{39}$$

where C_{eo} is a constant, and $\dot{y}_{b_{imp}} - \dot{y}_{o_{imp}}$ denotes $\dot{y}_b - \dot{y}_o$ at the instant when the collision occurs between the object and the endeffector.

Next, on the object, F_{men}^{s}(13), F_{He}^{s}(16), F_{dam}^{s}(17), F_{men}^{e}(36), F_{He}^{e}(37), and F_{dam}^{e}(38) are exerted. Therefore, F_o is given by:

$$F_o = F_{He}^{s} + F_{dam}^{s} + F_{men}^{s} - F_{He}^{e} - F_{dam}^{e} - F_{men}^{e}. \tag{40}$$
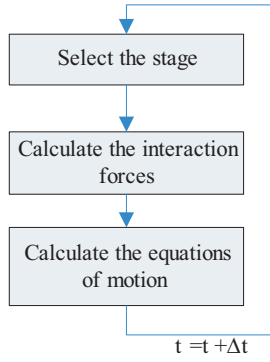
(f) Contact-diving stage

Fig. 7. Flow cart for numerical solution procedure

On the endeffector, F_{men}^e(36), F_{He}^e(37), and F_{dam}^e(38) are exerted. On the object, F_{liq}^s(27), F_{men}^e(36), F_{He}^e(37), and F_{dam}^e(38) are exerted. Therefore, F_b and F_o are given by:

$$F_b = F_{He}^e + F_{dam}^e + F_{men}^e. \tag{41}$$
$$F_o = -F_{liq}^s - F_{He}^e - F_{dam}^e - F_{men}^e. \tag{42}$$

Based on this analysis, we consider to simulate the dynamical motion of the endeffector and the object. Fig.7 shows the flow chart for the numerical solution procedure. First, according to $h_{l_{eo_c}}$, $h_{l_{os_c}}$, and r_2, we deicide which stage the system is belonging to, at t (note that r_2 is used when judging whether the endeffector/object is at flying or diving stage. when r_2 becomes zero, the endeffector/object is judged to come into flying stage). Next, we calculate F_b and F_o. Third, substituting the calculated F_b and F_o into (1) and (2), we calculate the dynamical motion of the endeffector and the object. Forth, we go next time step ($t = t + \Delta t$). Iterating the above steps, we can calculate the dynamical motion of the endeffector and the object.

IV. RESULTS FOR SIMULATION AND EXPERIMENT

To show the validity of our approach, we show some simulation results and some experimental results.

First, the simulation setting is described.
• The parameter values for the simulation are listed in the above nomenclatures.
• Practically, pizocell is driven by voltage. The relationship between the bending moment produced from pizocell, M_p, and the input voltage to the pizocell, V_{in}, is given by:
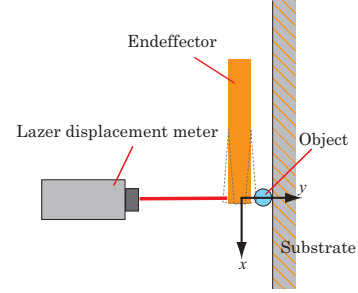
$$M_p = k_{mv} V_{in}. \tag{43}$$

where k_{mv} is a constant value derived based on the theory of elasticity [11]. We set V_{in} as follows:

$$V_{in} = V_{amp} \sin(\omega t). \tag{44}$$

where V_{amp} is the amplitude of the input voltage. ω is set to 22607[rad/sec], which corresponds to the forth mode frequency of the endeffector. The value of ω is theoretically
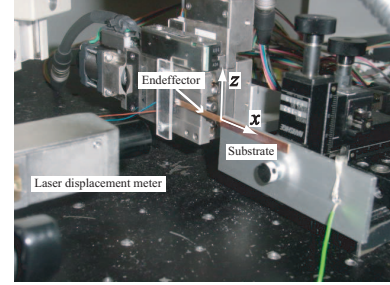

(a) Photo of the experimental set up

(b) The overview of the experimental set up

Fig. 8. Experimental set up for investigating the endeffector motion

calculated. The initial value of y_b is set to 0[m], and the initial value of y_o is set to $y_s - r_0$. We simulated in the case where V_{amp} is 5, 10, and 20[V].
• Eq. (1) can be solved by introducing the discrete variable method and applying Duhamel integral [11].
• In the calculation of P produced from (5), we employed the finite difference method based on the divergence formulation method, direct simulation of the flow conservation, and the Newton-Raphson linearization method. The nodal points for the calculation are set to 50, equally spaced along the r coordinate.
• The Poiseuille flow rate coefficient, $Q_p(D, \alpha)$, are calculated, using the database produced by Fukui and Kaneko [13].
• We simulated the following case: First, we oscillate the endeffector freely. Then, at $t = 0.0121$, we approach the endeffector to the object on the substrate.
• The sampling time is set to $0.5[\mu sec]$. Considering hysteresis, C_{eo} in (39) is set to 1 for $\dot{y}_{b_{imp}} - \dot{y}_{o_{imp}} > 0$ and 10 for $\dot{y}_{b_{imp}} - \dot{y}_{o_{imp}} < 0$. Similarly, C_{os} in (18) is set to 1 for $\dot{y}_{o_{imp}} > 0$ and 10 for $\dot{y}_{o_{imp}} < 0$.

Fig.8 shows the experimental set up. This system consists of the manipulation system, the image-capturing system, the finger-oscillating system, and the displacement measuring system. The manipulation system consists of the endeffector (pushing finger), the substrate, and the object. The endeffector is a copper cut in size of $40 \times 3 \times 0.3$mm. On the endeffector, the piezocell (FUJI CERAMICS C6) of $4 \times 3 \times 0.3$mm is bonded as an actuator for oscillating it. The endeffector is attached on the XYZ stage (PMZG413 SURUGASEIKI)
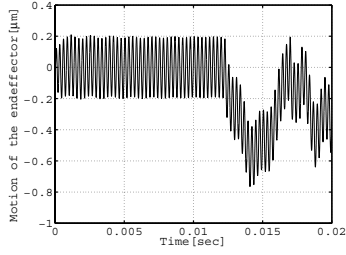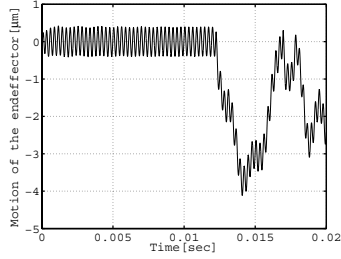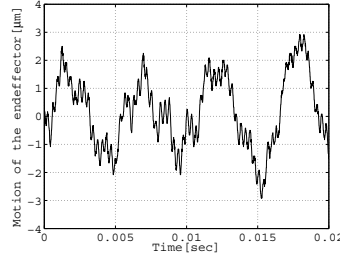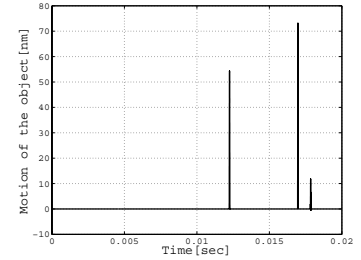
(a) $V_{amp} = 5$ V
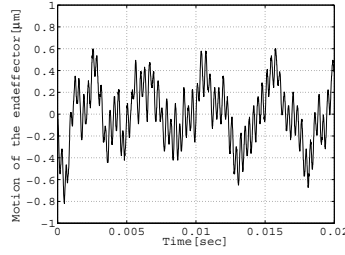
(a) $V_{amp} = 5$ V
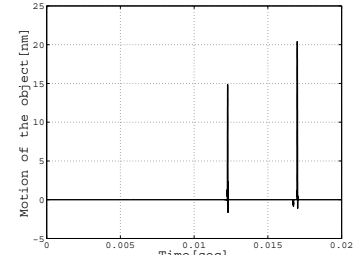
(a) $V_{amp} = 5$ V

(b) $V_{amp} = 10$ V

(b) $V_{amp} = 10$ V
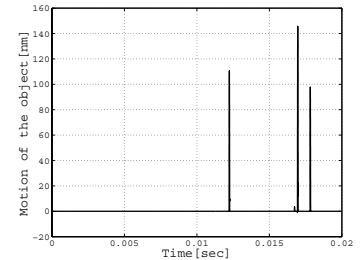

(b) $V_{amp} = 10$ V
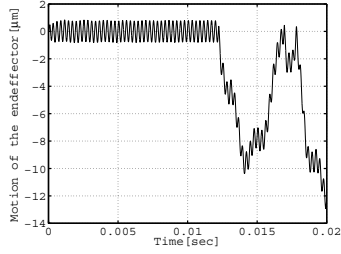
(c) $V_{amp} = 20$ V
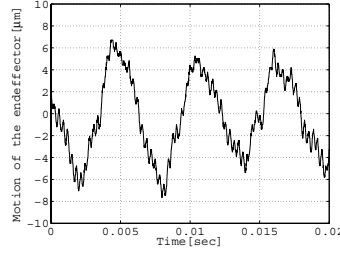
(c) $V_{amp} = 20$ V

(c) $V_{amp} = 20$ V

Fig. 9. The endeffector motion (simulation results)

Fig. 10. The endeffector motion (experimental results)

Fig. 11. The object motion (simulation results)

which can be controlled by PC. The substrate is also a copper cut. The endeffector and the substrate are grounded for preventing an extra charge. The object is a glass sphere (UNION, unibeads) with a radius of 97[μm]. The image-capturing system is for recording the movie of the motion of the endeffector and the object. The motion is captured by the CCD camera (IAI, CV-S3200) through the microscope (MORITEX, ML-Z07545). The captured data is send to PC through the capture board (V-STREAM, VS-TV2800R). The oscillation of the endeffector is generated by oscillating the piezocell by the function generator (YOKOGAWA, FG120) through the power amplifier (NF, 4010). The displacement of the endeffector is measured by the laser displacement meter (SONY, VL10). Note that the laser displacement meter can measure only a relative displacement. The frequency is set to 3.136 [kHz] which corresponds to 3rd mode frequency of the endeffector. The input signal is a sine curve. We measured in the case where the amplitude of the input voltage is 5, 10, and 20 [V].

Fig.9 and Fig.11 respectively show the calculated motions of the endeffector and the objects in the simulation.

Fig.10 shows the measured displacement of the endeffector. At every case, the endeffector contacts with the object. Note that when the endeffector freely vibrates, the amplitude is about 0.2[μm] at 5[V] of V_{amp}, about 0.4[μm] at 10[V] of V_{amp}, and about 0.8[μm] at 20[V] of V_{amp}.

Comparing with Fig.9 and Fig.10, we can see that the calculated wave form resembles the measured wave form. The amplitude of the calculated wave form is almost same as the amplitude of the measured wave form. The period of the calculated wave form is also almost same as the period of the measured wave form. Then, we can show the validity of our theoretical model and the simulation.

From Fig.9 and Fig.10, we can see that; (1) Comparing with

the case where the endeffector freely vibrates, the amplitude becomes very large in the case where the endeffector interacts with the object. (2) In the case where the endeffector interacts with the object, the oscillation is disturbed by the collision, and the lower order mode oscillation is excited. Therefore, the average period changes. (3) The amplitude of the oscillation increases with the increase of the input voltage. It is because the velocity magnitude at the collision increases with the increase of the input voltage.

From Fig.11, we can see that the object is not removed from the substrate when the oscillating endeffector approaches to the object on the substrate. Namely, the oscillation of the endeffector can reduce the adhesion effect between the endeffector and the object, attracting the object to the substrate. One of the reason why the object is not removed is considered to be for the damping force resulted from the liquid lubricant (refer to (27)). When the object tries to be removed from the substrate, not only the meniscus force but also the damping force attract the object to the substrate. We can also see that the object is compressed on the substrate. Especially, the object is deeply compressed around when the collision occurs between the endeffector and the object. Note that in the experiment, we can not measure the object motion because of the configuration of the endeffector, the object, and the substrate (and the laser displacement meter). Using the simulation, we can estimate the object motion.

V. CONCLUSION

In this paper, we have analyzed the mechanism of the phenomenon between an endeffector, a micro object, and a substrate, when the oscillating endeffector approaches to the micro object on the substrate. In a micro range, the attracting forces such as the van der Waals, capillary, and electrostatic forces dominate. Therefore, the adhesion occurs between the endeffector and the object during the micro manipulation. Then, it is hard to complete the micro manipulation. Recently, we proposed the method to reduce the adhesion effect [10]. When bringing an oscillating endeffecter close to a micro object on a substrate, the attracting force between the object and the endeffector is reduced, attracting the object to the substrate. Then, it becomes easy to remove the endeffector from the object. However, the mechanism was unclear. In this paper, we have derived a theoretical model of the phenomenon, and simulate the dynamical motion of the endeffector and the object. Comparing the simulation results and the experimental results, we show the validity of our approach. From the simulation results and the experimental results, we show that the oscillation of the endeffector can reduce the adhesion effect between the endeffector and the object, attracting the object to the substrate.

REFERENCES

[1] R. S. Fearing, "Survey of sticking effects for micro-parts," *Proc. of the IEEE/RSJ International Conference on Intelligent Robots and Systems*, pp. 212–217, 1995.

[2] F. Arai, D. Andou, and T. Fukuda, "Micro Manipulation Based on Physical Phenomena in Micro World (1st Report, The Reduction Method of Van Der Waals Force)," *Transactions of the Japan Society of Mechanical Engineers, Series C*, vol. 62, no. 603, pp. 4286–4293, 1996, (in Japanese).

[3] F. Arai, D. Andou, Y. Nonoda, and T. Fukuda, "Micro Manipulation Based on Physical Phenomena in Micro World (Principle and Prototype Experiments of Adhesion-type Micro Endeffector)," *Transactions of the Japan Society of Mechanical Engineers, Series C*, vol. 62, no. 604, pp. 4630–4635, 1996, (in Japanese).

[4] W. Zesch, M. Brunner, and A. Weber, "Vacuum tool for handling micro objects with a nano robot," *Proc. of the IEEE International Conference on Robotics and Automation*, pp. 1761–1766, 1997.

[5] Y. Rollot, S. Régnier, and J. Guinot, "Dynamical model for the micro-manipulation by adhesion : Experimental validations for determined conditions," *Journal of Micromechatronics*, vol. 1, no. 4, pp. 273–297, 2002.

[6] D. S. Haliyo, Y. Rollot, and S. Régnier, "Manipulation of micro-objects using adhesion forces and dynamical effects," *Proc. of the IEEE International Conference on Robotics and Automation*, pp. 1949–1954, 2002.

[7] D. S. Haliyo and S. Régnier, "Advanced applications using [$m\ddot{u}$]mad, the adhesion based dynamic micro-manipulatior," *Proc. of the IEEE/ASME International Conference on Advanced Intelligent Mechatronics*, pp. 880–885, 2003.

[8] S. Saito, H. T. Miyazaki, T. Sato, K. Takahashi, and T. Onzawa, "Analysis of micro-object operation considering the dynamics considering the adhesion under an sem," *Proc. of the IEEE/RSJ International Conference on Intelligent Robots and Systems*, pp. 1349–1357, 2001.

[9] S. Saito, H. Himeno, and K. Takahashi, "Electrostatic detachment of an adhering particle from a micromanipulated probe," *Journal of Applied Physics*, vol. 93, no. 4, pp. 2219–2224, 2003.

[10] T. Watanabe, N. Fujino, and Z. Jiang, "Micromanipulation using squeeze effect," *Proc. of IEEE/RSJ International Conference on Intelligent Robots and Systems*, pp. 3357–3362, 2004.

[11] Z. W. Jiang, S. Chonan, and J. Tani, "Tracking control of a miniature flexible arm using piezoelectric bimorph cells," *The International Journal of Robotics Research*, vol. 11, no. 3, pp. 260–267, 1992.

[12] S. Fukui and R. Kaneko, "Analysis of ultra-thin gas film lubrication based on linearized boltzmann equation: First report-derivation of a generalized lubrication equation including thermal creep flow," *Transaction of the ASME, Journal of Tribology*, vol. 110, pp. 253–262, 1988.

[13] ——, "A database for interpolation of poiseuille flow rates for high knudsen number lubrication problems," *Transaction of the ASME, Journal of Tribology*, vol. 112, pp. 78–83, 1990.

[14] J. N. Israelachvili, *Intermolecular and Surface Forces, 2nd ed.* Academic, New York, 1992.

[15] K. Okuyama, H. Masuda, K. Higashitani, M. Chikazawa, and T. Kanazawa, "Interaction between 2 particles," *Journal of the Society of Powder Technology*, vol. 22, no. 7, pp. 27–51, 1985, (in Japanese).